IEEE Open Journal of
Antennas and Propagation

Received 5 June 2023; revised 28 July 2023; accepted 4 August 2023. Date of publication 9 August 2023; date of current version 29 August 2023.

Digital Object Identifier 10.1109/OJAP.2023.3303468

Analysis and Experimental Demonstration of Reflectarray Antennas in Quasi-Regular Lattices

BORJA IMAZ-LUEJE [1] (Student Member, IEEE), JUAN CÓRCOLES [2] (Senior Member, IEEE), MARCOS R. PINO [1], AND MANUEL ARREBOLA [1] (Senior Member, IEEE)

[1]Department of Electrical Engineering, Group of Signal Theory and Communications, Universidad de Oviedo, 33206 Gijón, Spain

[2]Department of Electronic and Communication Technology, Escuela Politécnica Superior, Universidad Autónoma de Madrid, 28049 Madrid, Spain

CORRESPONDING AUTHOR: M. ARREBOLA (e-mail: arrebola@uniovi.es)

This work was supported in part by MCIN/AEI/10.13039/501100011033 under Grant PID2020-114172RB-C21, Grant PID2020-116968RB-C32, Grant TED2021-130650B-C21, and Grant TED2021-130650B-C22, cofounded by European Union (UE) "NextGenerationEU"/PRTR; in part by the Gobierno del Principado de Asturias under Project AYUD/2021/51706; and in part by the Ministerio de Educación y Formación Profesional under Grant FPU18/0257.

ABSTRACT This paper presents investigations on reflectarray antennas using non-periodic element distributions. The study involves the analysis and design of two reflectarrays based on quasi-periodic lattices with rectangular and pentagonal profiles, whose performance is compared with equivalent reflectarrays comprised of regular grids of elements. The characterization of these antennas is performed using a tailored analysis technique for reflectarrays with periodical and quasi-periodical grids. The proposed technique uses the Method of Moments under local periodicity conditions (MoM-LP) to compute the field on the surface of each cell and then the far field radiated by the aperture. In both aperture profiles, the quasi-periodic lattices are designed to provide an optimal adjustment, with the edge of the reflectarray maintaining an inter-element spacing similar to the regular grids of elements. This is particularly useful in non-canonical profile apertures, where the regular lattices do not adjust properly with the shape of the reflectarray and therefore exhibit less control of the reflected field in the aperture. The reflectarrays comprised of quasi-regular lattices achieve similar performance in terms of beam shaping, SLL and crosspolar discrimination to those based on regular grids. However, they show an improvement in fractional bandwidth between 7.4% and 11.3%.

INDEX TERMS Reflectarray antenna, quasi-periodic surfaces, triangular lattice, non-regular lattice.

I. INTRODUCTION

THE USE of periodic surfaces has aroused great interest within the scientific community. In addition to the most mature technologies such as arrays, several types of spatial fed surfaces have been used in many microwave systems. This group includes metasurfaces [1], [2], reflectarrays [3], [4], [5], transmitarrays [6], [7], [8], [9], or Frequency Selective Surfaces (FSS) [10], [11], among others. In particular, spatial fed arrays such as reflectarrays or transmitarrays have been proposed as potential candidates in various applications, such as satellite communications [5] or cellular networks [7], [10].

The elements on a periodic surface are usually distributed in a rectangular lattice [1], [2], [3], [4], [5], [6], [7], [8], [9], [10], [11]. However, this distribution does not fit optimally on surfaces with non-rectangular profiles or shapes. In order to overcome this limitation, the periodicity can be reduced and sub-wavelength reflective metasurfaces can be employed. As an alternative, several works propose the use of periodic surfaces based on a triangular regular lattice [12], [13], [14], [15]. Such lattices allow for increasing the density of the elements and maintaining the inter-element spacing, which improves the performance of the antenna in terms of side lobes reduction and bandwidth. Furthermore, sub-wavelength and triangular lattices enable a better adjustment to arbitrary shapes, although this adaptability is still limited in the case of conformal surfaces.

In line with this, quasi-periodic surfaces exhibit more potential flexibility to adapt to an arbitrary shape. They are composed of a lattice where the distance between

This work is licensed under a Creative Commons Attribution 4.0 License. For more information, see https://creativecommons.org/licenses/by/4.0/

elements varies in a small range along the surface. The use of quasi-periodic surfaces in array antennas has been proposed to improve certain parameters of a conventional array, such as bandwidth and side radiation. Among the different types of quasi-periodic surfaces, it is worth mentioning those whose elements distribution is obtained from optimization [16], [17], [18], [20] or those generated by analytical expressions [20], [21], [22]. Particularly in reflectarrays, [16], [20] presents a synthesis procedure in which the position of the elements is considered as a degree of freedom in the algorithm to improve the performance of the shaped-beam pattern. In [22], a circular shape reflectarray antenna whose elements are distributed in a log-spiral lattice is presented. This reflectarray structure achieves higher gain and lower side lobe levels in comparison with other types of lattices. To the best of the authors' knowledge, the use of quasi-periodic lattices in reflectarrays has been focused on the improvement of different electrical parameters of the antenna but not on the capabilities of such lattices to adapt to an arbitrary reflectarray profile. This could be of interest in antenna configurations that require reflectors with non-canonical shapes, as reported in [23], [24], [25], [26].

During the analysis of periodic or quasi-periodic reflectarrays, the study of the unit cell is a critical point. It is usually performed under local periodicity conditions, using full-wave methods such as MoM [27], [28], Finite Element Method (FEM) [8], or Finite Difference Time Domain FDTD [9], among others. The use of one or the other method responds to a trade-off between flexibility in the geometries to be analyzed, accuracy in the achieved results, and computation time [29]. Once the behavior of the cell is known, the most common methods for the calculation of the field radiated by the structure are the integration of the field aperture [30], the principle of superposition [31], or array theory [32]. The former method is typically implemented through efficient algorithms such as the Fast Fourier Transform (FFT) for periodical surfaces [3] and the Non-Uniform FFT (NUFFT) on aperiodic surfaces [19], [33], [34].

This contribution presents a theoretical and experimental study on the use of quasi-regular lattices in reflectarrays designed to adjust properly to different aperture profiles. For this purpose, a tailored technique to analyze and design reflectarrays with a regular or quasi-regular element distribution is introduced. It uses a MoM-based method for the analysis of the field in the reflectarray surface under different periodicity conditions. Different subdivisions of the reflectarray aperture are used to calculate the radiated field, depending on the unit-cell arrangement. Using this technique, two reflectarray examples with different aperture profiles (rectangular and pentagonal) have been designed and assessed. They are composed of a quasi-regular lattice of elements, generated through a triangulation algorithm that adapts the placement of the cells according to the reflectarray shape. The performance of both antennas is compared with two equivalent reflectarrays based on regular rectangular and regular triangular lattices. In addition, the rectangular

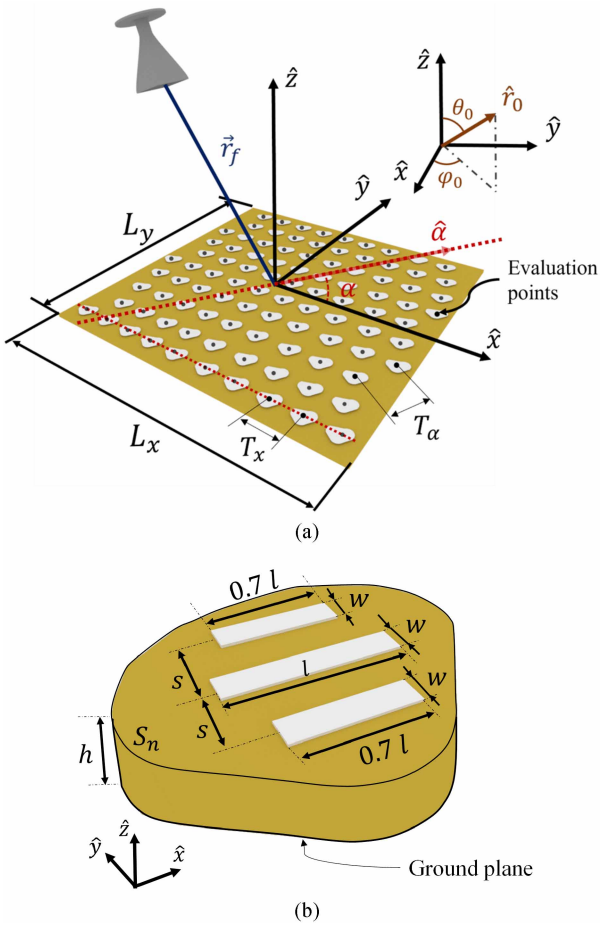

FIGURE 1. Sketch of the reflectarray surface: (a) Geometry of the periodical reflectarray surface. (b) Detail of the unit-cell.

reflectarray based on a quasi-regular lattice and its equivalents have been manufactured and experimentally tested. The results show that there is good agreement between the predicted and tested antenna performance, validating the proposed technique. In both reflectarray profiles, the use of quasi-regular grids exhibits similar performance compared to regular lattices, but with an enhancement in the antenna bandwidth. Moreover, the use of quasi-regular lattices in non-canonical shapes can lead to improvements in certain antenna features, such as a higher density of elements or in the gain of the antenna.

II. ANALYSIS OF REFLECTARRAYS WITH QUASI-REGULAR LATTICES

The radiated far field for a reflectarray is achieved based on the aperture theory [30]. Let us consider the scheme of Fig. 1(a) in which the reflectarray aperture is placed in the XY plane, with $+z$ being the propagation axis. Applying the Second Principle of Equivalence [30], the radiated field $\vec{E}$ is calculated as:

$$\vec{E}(\vec{r}) = -j\omega\eta_0\left[-\frac{\varepsilon_0}{4\pi r}\exp(-jk_0 r)\hat{z}\times\vec{P}(\hat{r})\right]\times\hat{r}, \qquad (1)$$

where ω is the angular frequency in vacuum; η_0=120π Ω is the vacuum impedance; ε_0 the electrical permittivity in vacuum; k_0 is the propagation constant in vacuum; $\vec{r}(r,\theta,\varphi)$ and $\widehat{r}(\theta,\varphi)$ indicates the direction of propagation in spherical coordinates; and $\vec{P}(\widehat{r})$ is the spectrum function, which is achieved as the surface integral of the tangential field $\vec{E}_a$ in the aperture surface S_a:

$$\vec{P}(\widehat{r}) = \iint_{S_a} \vec{E}_a(\vec{r}') \exp\left(jk_0\widehat{r}\cdot\vec{r}'\right) dS'. \tag{2}$$

According to this expression, the computation of the spectrum function requires two processes: (a) the knowledge of the tangential fields $\vec{E}_a(\vec{r}')$; and (b) the integration of these fields along the reflecting surface. The subsequent subsections provide a further discussion about these two aspects.

A. EVALUATION OF THE FIELD IN THE REFLECTARRAY SURFACE

The tangential field can be calculated numerically at a specific set of points $\vec{E}_a(\vec{r}_n)$, with $\vec{r}_n$ being the position vector of each n-th point regarding the reflectarray coordinate system. Based on [35], this set of points is arranged in a certain lattice as shown in Fig. 1(a). Such a lattice is periodic along two axes ($\widehat{x}$ and $\widehat{\alpha}$) that forms an angle α between them. The distance between points along these axes is T_x and T_α respectively. The tangential field reflected by the reflectarray can be obtained at each evaluation point, according to the following expression:

$$\vec{E}_a(\vec{r}_n) = \boldsymbol{R}_n\vec{E}_i(\vec{r}_n) = \begin{pmatrix} \rho_n^{XX} & \rho_n^{XY} \\ \rho_n^{YX} & \rho_n^{YY} \end{pmatrix} \vec{E}_i(\vec{r}_n), \tag{3}$$

where $\vec{E}_i(\vec{r}_n)$ is the incident field in the n-th point; and $\boldsymbol{R}_n$ is the matrix of reflection coefficients, which fully characterizes the behavior of the reflectarray surface. The elements of this matrix can be classified into direct coefficients (ρ_n^{XX} and ρ_n^{YY}) and cross-coefficients (ρ_n^{XY} and ρ_n^{YX}). In general, the field evaluation points coincide with the centers of the unit-cells of the reflectarray, so the $\boldsymbol{R}_n$ matrix quantifies the behavior of each unit-cell.

The computation of the matrix $\boldsymbol{R}_n$ is carried out under the assumption of local periodicity. In other words, the periodic grid is assumed to be infinite, and therefore the lattice arrangement is considered through the two discrete spectral variables $k_x^{n_x}$ and $k_y^{n_\alpha,n_x}$, defined as [35]:

$$k_x^{n_x} = k_0\sin\theta\cos\varphi + n_x\frac{2\pi}{T_x}, \tag{4a}$$

$$k_y^{n_\alpha,n_x} = k_0\sin\theta\sin\varphi + n_\alpha\frac{2\pi}{T_\alpha\sin\alpha} - n_x\frac{2\pi}{T_x\tan\alpha}, \tag{4b}$$

where n_x, n_α are the index that identifies the n-th element in each one of the periodical axes. To achieve reasonable computational times that enable full-wave design, an accurate and efficient method for the unit-cell analysis must be used. In this work, the unit-cell analysis is carried out through a dedicated in-house spectral-domain MoM for multilayered structures [36]. Since the unit-cell elements to be designed consist of printed metallic dipoles (see Section IV and Fig. 1(b)), electric currents in these dipoles are amenable to be approximated by entire-domain basis functions that properly model spatial edge singularities [37], and thus a reduced number of basis functions can be considered in the MoM while retaining accuracy. Furthermore, for these rectangular shapes, the Fourier transform can be computed analytically, rendering the spectral-domain MoM implementation highly efficient and making it possible to consider seamlessly different values of the spectral variables (4) for different lattice arrangements.

The reflectarrays presented in this work are comprised of the different lattices depicted in Fig. 2: Regular Rectangular Lattice (RRL), Regular Triangular Lattice (RTL), and Quasi-regular Triangular Lattice (QTL). The unit-cell analysis is performed by applying the formulation reported in [36] and the calculation of the spectral functions $k_x^{n_x}$ and $k_y^{n_\alpha,n_x}$, considering the features of each grid of elements.

The RTL (see Fig. 2(a)) consists of an equispaced element distribution, where the periodic axes are perpendicular ($\alpha = 90°$), fulfilling that $T_x = d_x; T_\alpha = d_y$. In the RTL shown in Fig. 2(b), the elements are arranged uniformly in an equilateral triangular pattern, with $\alpha = 60°$ and $T_x = T_\alpha = d$. Finally, the QTL (see Fig. 2(c)) has a quasi-periodic element arrangement, that is similar to the RTL case (the light blue points in Fig. 2(c) are distributed as an equivalent regular triangular lattice and the black ones show the location of the points in the quasi-regular grid). This scheme considers $\alpha = 60°$ and the inter-element spacing $T_x = T_\alpha = \widetilde{d}_n$, being $\widetilde{d}_n$ the mean distance from each element to the four nearest cells (distances $d_{1n},\ldots,d_{4n}$ depicted in Fig. 2(c)). Using (4), the spectral values $k_x^{n_x}$ and $k_y^{n_x,n_\alpha}$ take the values:

$$k_x^{n_x} = k_0\sin\theta\cos\varphi + n_x\frac{2\pi}{\widetilde{d}_n}, \tag{5a}$$

$$k_y^{n_\alpha,n_x} = k_0\sin\theta\sin\varphi + (2n_\alpha - n_x)\frac{2\pi}{\widetilde{d}_n\sqrt{3}}. \tag{5b}$$

Note that the spectral variables take the same expression in the RTL case, by replacing $\widetilde{d}_n$ by d.

B. COMPUTATION OF THE FIELDS IN THE REFLECTARRAY APERTURE

Once the reflected tangential field $\vec{E}_a(\vec{r}_n)$ on the surface has been calculated, the next step is the integration of the spectrum function $\vec{P}(\widehat{r})$. For this purpose, the aperture is divided into a set of sub-apertures, with each one having a uniform field equivalent to the evaluation points $\vec{E}_a(\vec{r}_n)$. Thus, equation (2) can be reformulated as:

$$\vec{P}(\widehat{r}) = \sum_{n=1}^{N_t} \vec{E}_a(\vec{r}_n)F(\widehat{r},n)\exp(jk_0\widehat{r}\cdot\vec{r}_n), \tag{6}$$

with N_t being the total number of evaluation points; and $F(\widehat{r},n)$ the amplitude of the element radiation pattern. This

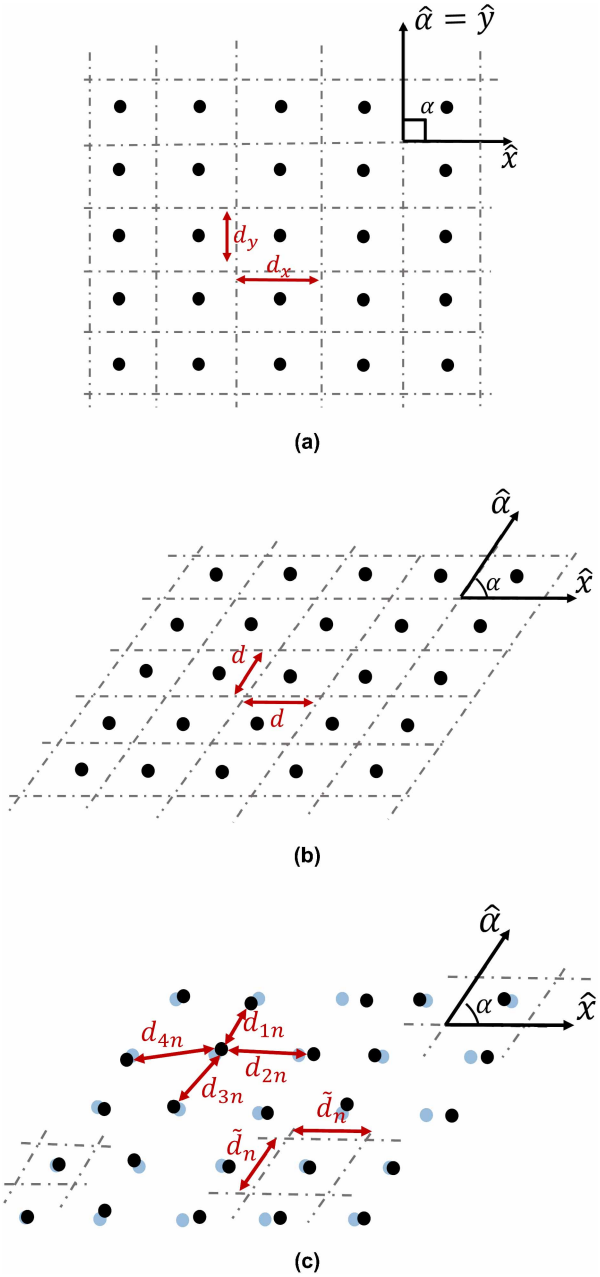

FIGURE 2. Distribution of the evaluation elements in the reflectarray aperture: (a) Regular Rectangular Lattice; (b) Regular Triangular Lattice; (c) Quasi-regular Triangular Lattice.

function can be achieved by surface integration in the domain of the n-th sub-aperture S_n (see Fig. 1(b)),

$$F(\widehat{r}, n) = \iint_{S_n} \exp\left(jk_0\widehat{r}\cdot\vec{r}'\right)dS_n'. \tag{7}$$

According to this expression, $F(\widehat{r}, n)$ relies on the shape of the sub-apertures, which is determined by the element arrangement. Fig. 3 illustrates the different sub-division of the reflectarray aperture for each element lattice (RRL, RTL, and QTL). For triangular grids of elements (RTL and QTL), the reflectarray aperture is discretized as a honeycomb mesh (see Fig. 3(b), (c)). The n-th sub-aperture in this case is a hexagon, whose apothem is $d/2$ and $\widetilde{d}_n/2$ in the RTL and QTL scenarios respectively. For simplicity, the hexagonal aperture is replaced by a circumference of radius $r_{d,n}$ (red circumference depicted in Fig. 3(b), (c)) with the same area. The change in cell aperture shape produces a small overlap between adjacent apertures with limited impact in the computation of the radiated power since the aperture size is kept. The function $F(\widehat{r}, n)$ in this case can be written as:

$$F(\widehat{r}, n) = \frac{2\pi r_{d,n}}{k_0 \sin\theta} J_1\left(k_0 r_{d,n}\sin\theta\right), \tag{8}$$

where $J_1(x)$ is the Bessel function of the first kind and order one. Note that in the RTL case, the radius of the circumference is equal in all sub-apertures ($r_{d,n} = r_d$) and therefore $F(\widehat{r}, n) = F(\widehat{r})$.

The computation of (5) can be done by direct evaluation of the sum or by applying efficient algorithms based on the Fourier transform. When the element arrangement is regular, such as in the RRL and RTL case, the Fast Fourier Transform (FFT) can be used [3], [19]. However, if a QTL is used, the computation of $\vec{P}$ cannot be obtained with the FFT. In these cases, it is possible to apply other algorithms such as the Non-Uniform FFT (NUFFT) as devised in [33], [34].

III. DESIGN OF REFLECTARRAYS WITH DIFFERENT LATTICES

Two examples of reflectarrays using QTL have been designed. One consists of a rectangular aperture (R-QTL), and the other of a pentagon-shape (P-QTL). The reflectarrays operate at 28 GHz, generating a pencil-beam pattern in single-linear polarization. Each QTL design will be compared with two equivalent reflectarrays that use an RRL and an RTL arrangement. The equivalents of the R-QTL are denoted as R-RRL and R-RTL. The equivalents of the P-QTL are denoted as P-RRL and P-RTL.

A. ANTENNA OPTICS

A perspective view of the antenna optics for reflectarrays with rectangular aperture is depicted in Fig. 1(a), while Table 1 lists the main optical characteristics of all reflectarray designs. They follow a single-offset configuration in which the reflectarray aperture is either a rectangle (see Fig. 1(a)) or a pentagon. The dimensions of the apertures (denoted by L_x and L_y along each axis) are 193.05 mm x 193.05 mm.

The distribution and number of radiating elements (N_t in Table 1) is different for each reflectarray design. Both R-RRL and P-RRL reflectarrays are formed by a square grid of 44 × 44 elements, considering an inter-element spacing in both axes ($d_x = d_y$ according to Fig. 2(a)) of 4.29 mm, which is $0.4\lambda_0$ at 28 GHz. The RTL designs are comprised of a triangular regular lattice as the one shown in Fig. 2(b), considering a $d = 0.4\lambda_0$. The regular grid in the P-RRL and P-RTL are properly trimmed according to the pentagonal shape of the aperture.

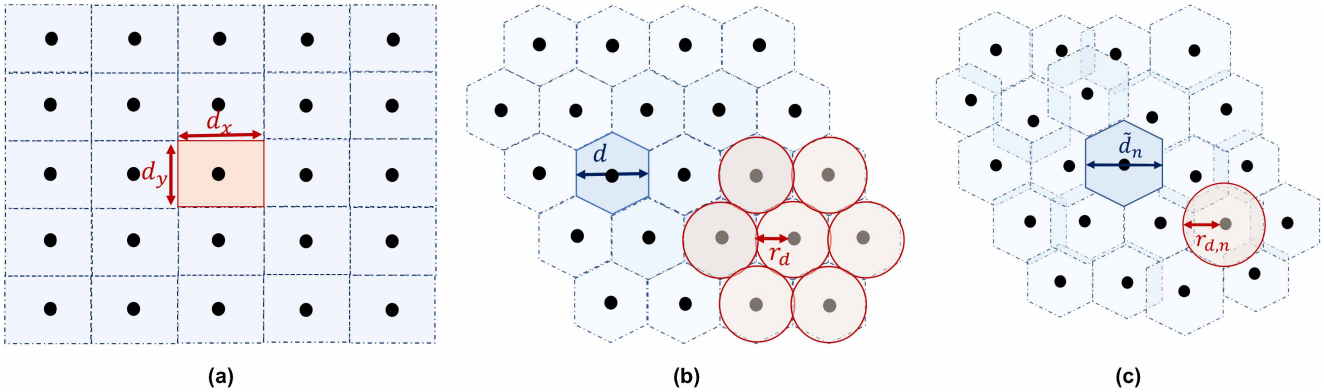

FIGURE 3. Division of the reflectarray aperture for each lattice: (a) Regular Rectangular Lattice; (b) Regular Triangular Lattice; (c) Quasi-regular Triangular Lattice. In blue, the equivalent aperture of each cell and in red the aperture considered during the analysis.

TABLE 1. Optics of the reflectarray designs.

	R-RRL	R-RTL	R-QTL	P-RRL	P-RTL	P-QTL
N_t	2025	2270	2226	1333	1533	1595
RA shape	Rectangle			Pentagon		
$L_x \times L_y$	193.05 mm x 193.05 mm					
$\vec{r}_f$	(-73.0, 0.0, 190.7) mm					
f/D	1.04					

The R-QTL and P-QTL are generated using an algorithm based on Delaunay triangulation [38], [39]. This algorithm is carried out considering the reflectarray profile (rectangular or pentagonal) as a constraint, and with a target inter-element spacing of 4.29 mm. Fig. 4 shows the normalized histogram of the mean distance between an element and its neighbors ($\tilde{d}_n$ in Fig. 2(c)) for both the R-QTL and P-QTL reflectarrays. Furthermore, it also depicts the distribution of these mean distances along the reflectarray aperture. The R-QTL reflector has a grid of elements that resembles a regular triangular lattice, where almost 80% of the inter-element spacings fall within the range of 4.29 $\pm$ 0.05 mm. The elements with $\tilde{d}_n$ outside this range are concentrated on the diagonals of the rectangular aperture. On the other hand, the P-QTL reflectarray features a more irregular grid of elements, with $\tilde{d}_n$ values scattered over a wider range of distances, although more than 60% of them are in the 4.29 $\pm$ 0.05 mm range. The inter-element spacing exhibits higher variability along the central and diagonals of the aperture, whereas in the different quadrants of the polygon, the element arrangement is nearly regular, similar to what is observed in the R-QTL case.

According to Table 1, the number of elements in the R-QTL reflectarray is almost the same as in the R-RRL case and slightly lower than in the R-RTL case (about 2% less). However, in the pentagonal reflectarray profile, the QTL provides a higher number of elements than in the other two regular grids. In particular, the P-QTL reflector has 20% and 4% more elements than the R-RRL and R-RTL designs, respectively.

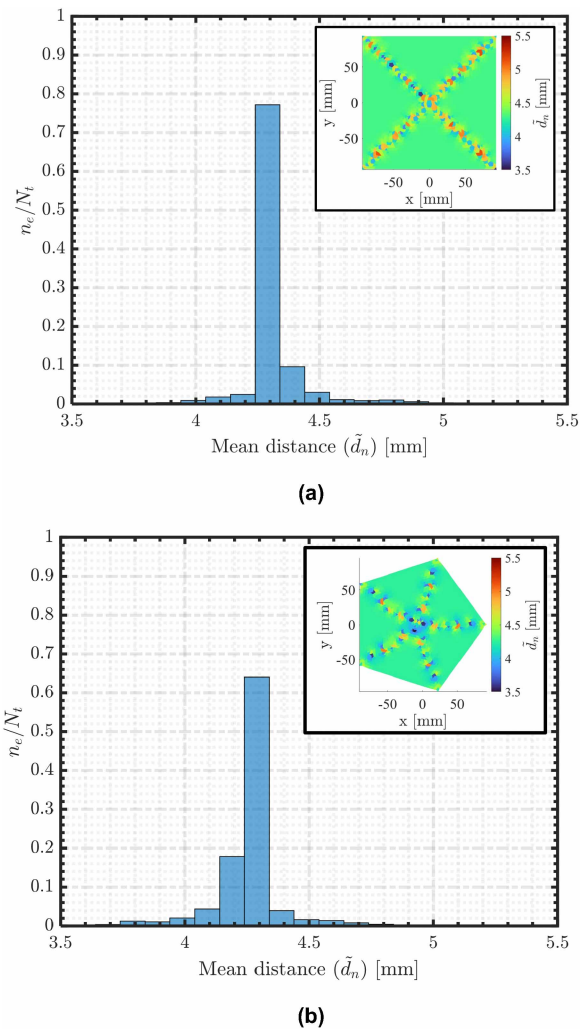

FIGURE 4. Normalized histogram of the mean distances per element ($\tilde{d}_n$) in the QTL reflectarrays and distribution of them along the aperture (northeast plots): (a) R-QTL; (b) P-QTL. The size of the bin in the histograms is 0.1 mm.

A Narda 665-20 pyramidal horn antenna is used to illuminate the different reflectarray designs. The phase center of the primary feed is located at the position $\vec{r}_f$ provided in

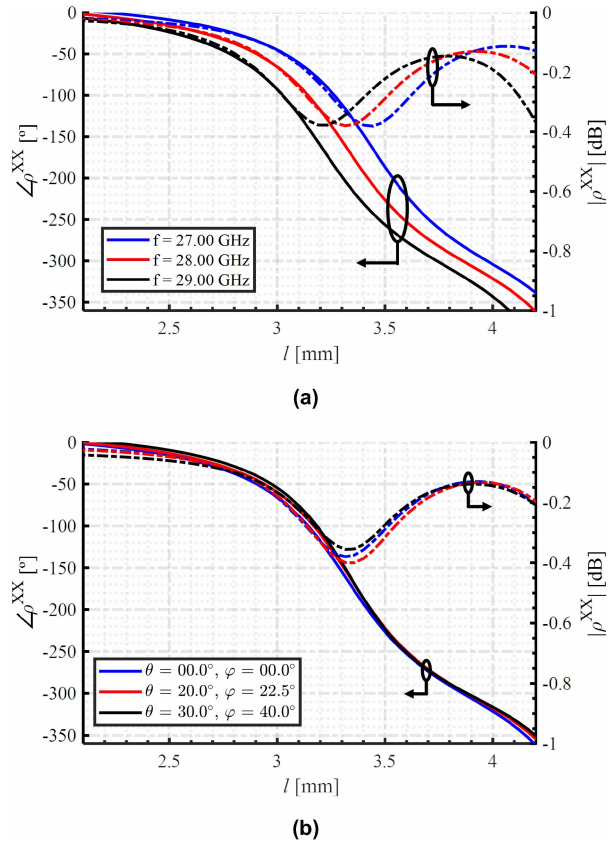

FIGURE 5. Unit cell used in R-RRL and P-RRL reflectarrays. Response of the direct coefficient ρ^{xx} in phase (right) and magnitude (left) as a function of the length of the dipole l considering: (a) different frequencies under normal incidence; (b) different angles of incidence at 28.0 GHz magnitude.

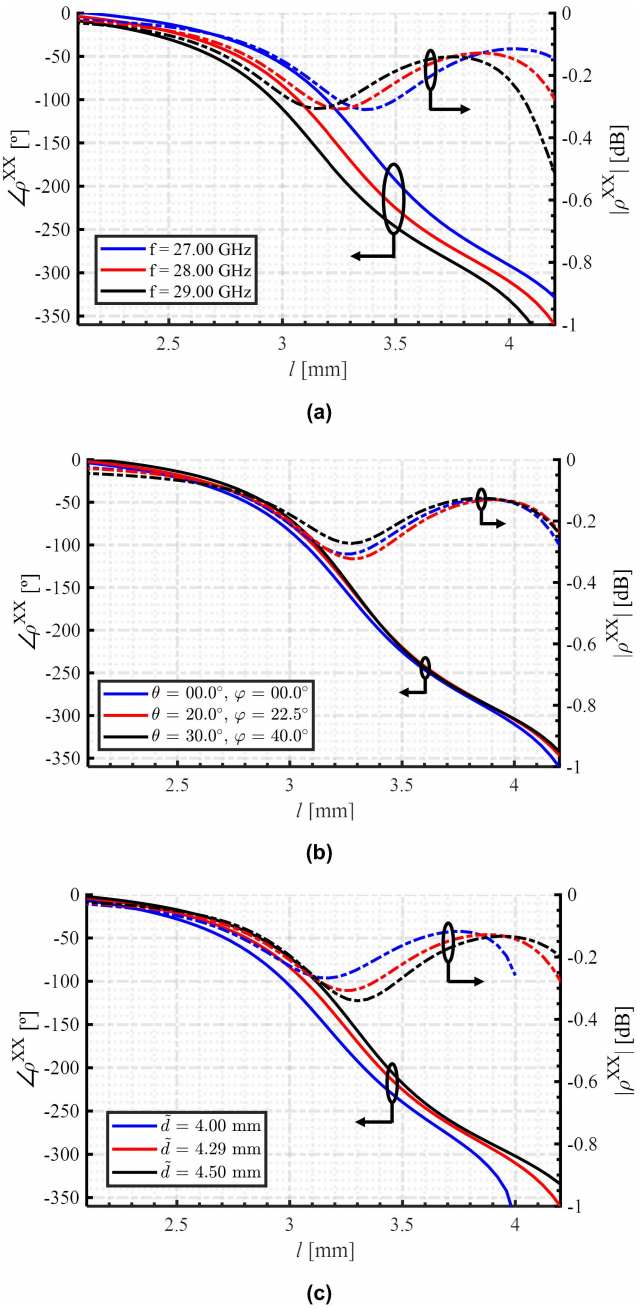

FIGURE 6. Unit-cell used in the R-RTL, R-QTL, P-RTL, and P-QTL reflectarrays. Response of the direct coefficient ρ_n^{xx} in phase (right) and magnitude (left) as a function of the length of the dipole l considering: (a) different frequencies under normal incidence; (b) different angles of incidence at 28.0 GHz; (c) different periodicities $\tilde{d}_n$ at 28.0 GHz under normal incidence.

Table 1, considering the coordinate system of Fig. 1(a). At the working frequency, the feed has a gain of 18.5 dBi. The subtended angle between feed and reflectarrays is 48.7°, so the pyramidal horn generates an average illumination taper at the edges of the reflector of 15 dB.

B. UNIT-CELL

Two configurations of unit-cells are used in the designs reported in this work: one for the RRL reflectarrays and the other for the RTL and QTL designs. Both configurations are composed of three metallic dipoles aligned with the x-axis of the reflectarray surface (see Fig. 1(b)). They are printed on the substrate diClad880 ($\varepsilon_r = 2.26, \tan\delta = 0.0025$) of thickness $h = 0.762$ mm. The width (w) of the dipoles is 0.5 mm and the ratio between the length of the lateral dipoles and the central one is 0.7. For the RRL designs, the distance between dipoles (s) is 1.43 mm while for the RTL and QTL reflectarrays is 1.2 mm. The shorter distance is chosen to avoid overlapping between dipoles of adjacent cells. Considering the analysis described in Section II-A, the cell topologies presented for each lattice have been assessed.

Fig. 5(a) and Fig. 6(a) show the reflection coefficient ρ^{XX} in each cell configuration when varying the length of the central dipole l under normal incidence. The cell topologies show a quasi-linear relationship between the phase-shift introduced by the element and the length of the dipole. Both cell topologies exhibit low in-band losses, below 0.6 dB, and good angular stability, as depicted in Fig. 5(b) and Fig. 6(b). Furthermore, Fig. 6(c) depicts the response of the cell for the different mean distance $\tilde{d}$ between 4 and 4.5 mm. This range covers the periodicity of more than 90% of the elements in both the R-QTL and the P-QTL reflectarrays (see Fig. 4). The phase response of

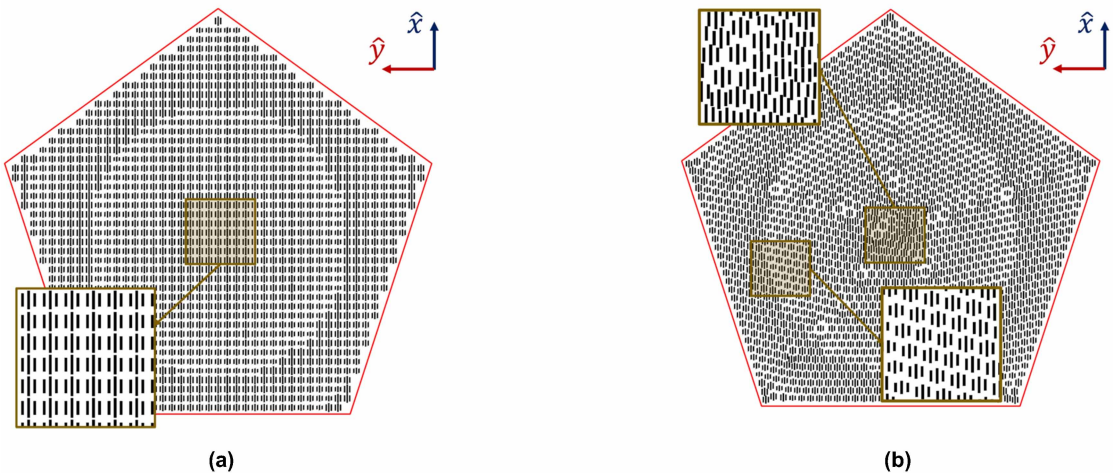

FIGURE 7. Layout of (a) the P-RRL and (b) the P-QTL reflectarrays. Solid red line indicates the edges of the reflectarray.

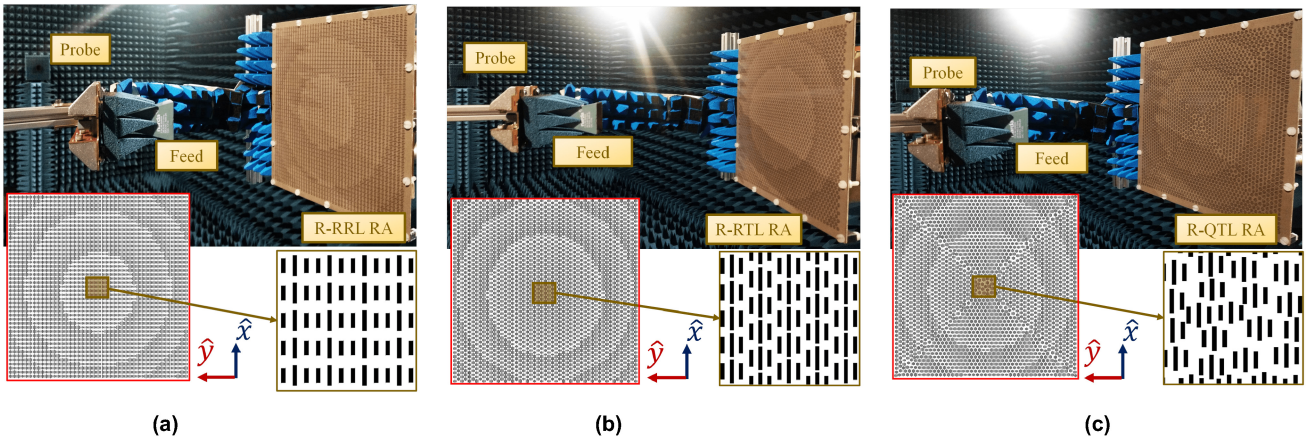

FIGURE 8. Layout of the rectangular reflectarrays and measurement setup used in their experimental validation: (a) R-RRL reflectarray; (b) R-RTL reflectarray; (c) R-QTL reflectarray.

the unit-cell exhibits little variations within this range of periodicities.

C. LAYOUT DESIGN PROCEDURE

Based on the optical scheme of Fig. 1(a), to generate a pencil beam in a certain direction of space $\widehat{r}_0(\theta_0, \varphi_0)$ each reflectarray element must introduce a phase-shift ϕ on its incident field, obtained as [3]:

$$\phi(\vec{r}_n) = k_0\left[r_{f,n} - (\vec{r}_n \cdot \widehat{r}_0)\right], \tag{9}$$

where $\vec{r}_n = (x_n, y_n)$ are the coordinates of the n-th element in the reflectarray coordinate system; and $r_{f,n}$ is the distance from the element to the phase center of the feed. For each reflectarray, the phase distribution $\phi(\vec{r}_n)$ is calculated using (8) and considering a beam-pointing direction $(\theta_0, \varphi_0) = (18.3°, 0.0°)$.

The phase distributions are used to determine the physical dimensions of the printed dipoles. This process is carried out element by element, adjusting the central dipole l properly to generate the phase response $\phi(\vec{r}_n)$. The unit cell is evaluated at 28 GHz using the analysis procedure described in Section II-A and the real incidence angle of the wave. In all reflectarray designs, it is considered a fixed inter-element spacing of 4.29 mm (i.e., $d_x = d_y = d = \widetilde{d}_n = 4.29$ mm). In the RRL and RTL designs, the length of the central dipole is limited to 4.27 mm due to manufacturing constraints, while in the QTL reflectarrays, the maximum dipole length is 3.8 mm to prevent overlapping between adjacent cells. The resulting layouts for the P-RRL and P-QTL cases are depicted in Fig. 7. The layout of the P-QTL approach exhibits a better adjustment with the pentagonal profile (red solid line depicted in Fig. 7) than in the P-RRL equivalent. Moreover, Fig. 8 presents the layouts of the three rectangular reflectarrays.

IV. NUMERICAL ANALYSIS OF REFLECTARRAYS BASED ON QUASI-REGULAR LATTICES

The evaluation of the quasi-regular reflectarrays and their equivalents was conducted using the procedure outlined in Section II. The incident field at each reflectarray aperture was obtained from the field at the feed aperture, using the GRASP software [40]. The $\boldsymbol{R}_n$ matrix was calculated with an in-house

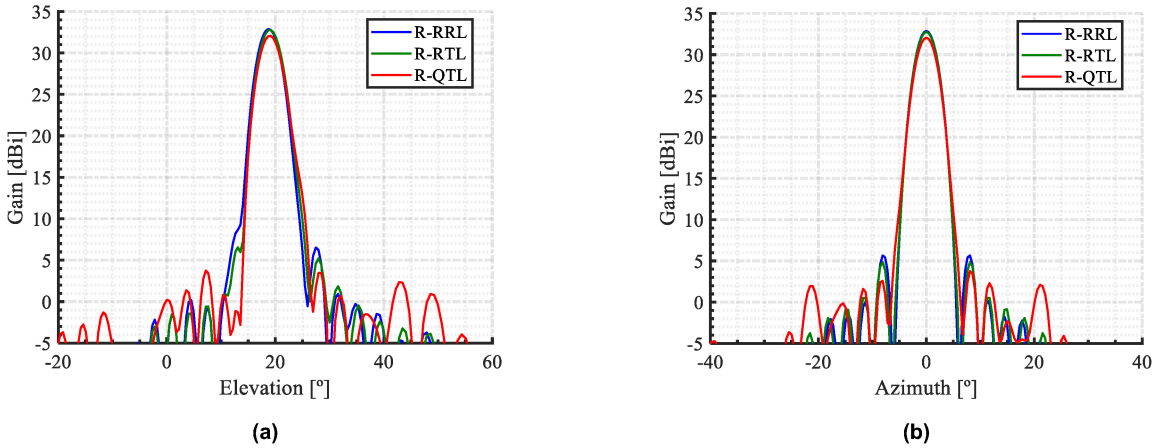

FIGURE 9. Simulated radiation pattern at 28 GHz of the reflectarrays based-on a rectangular shape: (a) Elevation cut $v = \sin(\theta_0)cos(\varphi_0)$; (b) Azimuth cut $u = \sin(\theta_0)cos(\varphi_0)$.

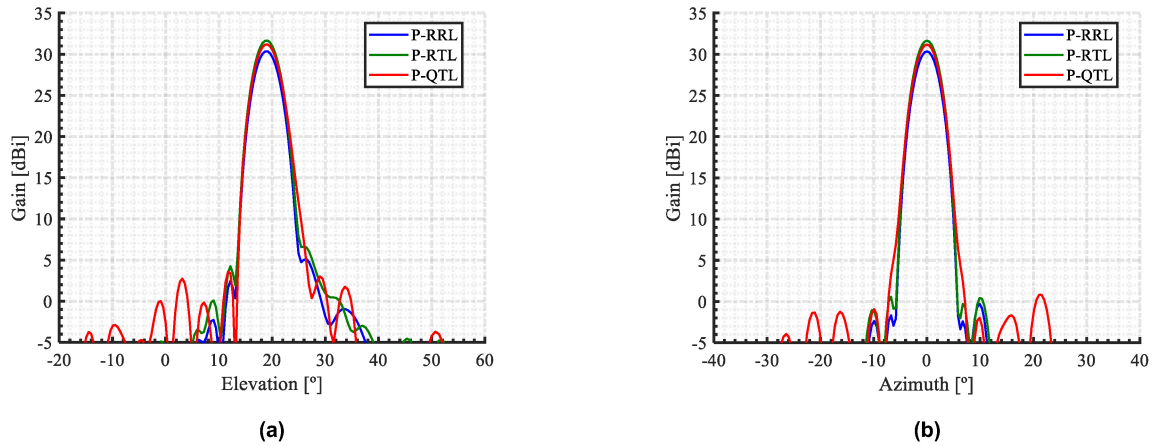

FIGURE 10. Simulated radiation pattern at 28 GHz of the reflectarrays based-on a pentagonal shape: (a) Elevation cut $v = \sin(\theta_0)cos(\varphi_0)$; (b) Azimuth cut $u = \sin(\theta_0)cos(\varphi_0)$.

MoM, as described in Section II-A. Then, the reflected field in the aperture was computed using (3), and the far field was calculated with (1) and (5). In the QTL designs, the mean periodicity of each radiating element $\widetilde{d}_n$ provided in Fig. 4 was considered during the unit-cell analysis and in the computation of (5).

A. QUASI-REGULAR RECTANGULAR REFLECTARRAY

Fig. 9 shows the radiation pattern of the rectangular reflectarrays at the design frequency. The R-QTL design generates a high-gain pencil beam pattern in the direction of design (θ_0, φ_0), with similar features as the R-RRL and R-RTL designs. It exhibits almost the same beam width, with slightly lower side lobe levels (SLL) and gain. More details about the performance of these three designs are discussed in Section V, where simulation results of these antennas are compared with measurements.

B. QUASI-REGULAR PENTAGONAL REFLECTARRAY

The pentagonal designs provide the radiation patterns depicted in Fig. 10 at 28 GHz. Table 2 also lists the main RF parameters of these three antennas assessed between 26 and 30 GHz.

The P-QTL reflectarray exhibits a similar radiation pattern to the P-RRL and P-RTL designs in terms of beamwidth and SLL, both at the design frequency and in-band. Table 2 also provides the cross-polar discrimination (XPD) calculated as the minimum difference between co- and cross-polar levels in an area of the main beam delimited by the 3dB drop of gain. The P-RTL design exhibits an XPD of around 30 dB, as their equivalents P-RRL and P-RTL. In terms of gain, the P-QTL design achieves gain levels 0.5 dB lower than the P-RTL case but 1 dB higher than the P-RRL reflectarray. Moreover, the reflectarray based on a quasi-regular grid exhibits more stability of gain in-band than the other two designs, as indicated by the 1 dB bandwidth (BW1dB parameter of Table 2, calculated considering the gain of the antennas at 28 GHz).

V. EXPERIMENTAL VALIDATION

The three rectangular reflectarray designs (R-RRL, R-RTL, R-QTL) have been manufactured and measured in the

TABLE 2. Simulated RF performance of the reflectarrays with pentagonal aperture.

		P-RRL Reflectarray					P-RTL Reflectarray					P-QTL Reflectarray				
Freq. [GHz]		26.0	27.0	28.0	29.0	30.0	26.0	27.0	28.0	29.0	30.0	26.0	27.0	28.0	29.0	30.0
SLL [dB]	Az.	-21.9	-28.9	-30.6	-26.8	-22.3	-22.2	-29.2	-31.1	-23.9	-21.6	-21.5	-27.8	-30.4	-23.7	-24.2
	El.	-21.5	-25.5	-25.2	-24.2	-31.8	-21.2	-25.1	-25.0	-27.3	-31.2	-20.9	-24.8	-27.6	-26.4	-21.6
XPD [dB]		31.4	30.9	30.7	29.9	29.5	30.5	31.2	30.6	30.3	29.8	31.2	31.0	30.6	30.4	29.6
Gain [dBi]		29.2	29.6	30.3	30.3	30.2	30.5	30.9	31.6	31.6	31.5	30.0	30.4	31.2	31.1	31.2
Eff [%]		51.1	51.9	56.7	52.9	48.3	68.9	70.1	76.5	71.4	65.1	61.4	62.4	69.8	63.5	60.8
BW1dB [GHz/%f_0]		4.4 / 15.7					4.5 / 16.1					7.0 / 25.0				

TABLE 3. Measured RF performance of the reflectarrays with rectangular aperture.

		R-RRL Reflectarray					R-RTL Reflectarray					R-QTL Reflectarray				
Freq. [GHz]		26.0	27.0	28.0	29.0	30.0	26.0	27.0	28.0	29.0	30.0	26.0	27.0	28.0	29.0	30.0
SLL [dB]	Az.	-22.5	-26.7	-26.8	-21.9	-18.9	-21.3	-23.2	-22.0	-21.0	-20.2	-22.8	-21.2	-21.8	-20.2	-19.4
	El.	-23.2	-23.1	-25.5	-21.0	-19.9	-22.2	-23.8	-30.7	-25.4	-22.6	-24.3	-22.7	-26.1	-21.1	-18.4
XPD [dB]		26.1	29.2	30.4	31.6	34.9	34.5	32.8	32.4	31.9	30.8	29.0	28.6	30.4	31.4	32.6
Gain [dBi]		31.5	32.4	33.0	32.5	32.3	31.9	32.6	33.2	33.2	33.4	31.1	31.9	32.2	32.1	32.1
Eff [%]		35.3	40.2	43.0	35.7	31.8	38.7	42.1	45.0	41.9	41.0	32.2	35.8	35.7	32.5	30.4

TABLE 4. Bandwidth predicted and measured in the rectangular reflectarray prototypes.

	Predicted	Measured
R-RRL	4.5 GHz / 15.7%	4.5 GHz / 15.7%
R-RTL	5.0 GHz / 17.9%	5.5 GHz / 19.6%
R-QTL	7.5 GHz / 27.0 %	7.5 GHz /27.0 %

facilities at the University of Oviedo. Fig. 8 shows the measurement setup employed. The layout of each design is placed in an aluminum supporting structure according to the antenna optics described in Section III-A. A dielectric ring frame at the edges of the reflectarrray breadboards are left to the proper assembly between the reflector and the supporting structure. Thus, the total area of each prototype is 205.92 mm x 205.92 mm.

The reflectarray demonstrators have been measured in a spherical range acquisition in an anechoic chamber. The probe of the setup, a standard gain Ka-band horn antenna, is located at 5 m for the Antenna Under Test (AUT). Since the probe is in the Fresnel zone of the reflectarrays under test, the far field is obtained by applying a near field to far field (NF-FF) transformation using the software SNIFT [41].

Fig. 11 shows the performance achieved both for measurements and simulation in a 4 GHz bandwidth and Table 3 provides the main features of these radiation patterns. An overall good agreement can be found between simulation and measurements in the three demonstrators, both at design frequency and in-band.

The experimental results of the R-QTL prototype align with the abovementioned simulations, revealing a copolar radiation pattern that is similar in shape to both R-RTL and R-RTL prototypes at the central frequency. Within the operating bandwidth, the R-QTL reflectarray maintains a high resemblance to the R-RTL reflectarray, but larger disparities appear in comparison to the R-RRL demonstrator, particularly in the stability of the main beam.

Table 3 lists the XPD calculated following the procedure explained in Section IV-B. The R-QTL prototype achieves lower XPD values than the other two prototypes, although such levels remain below 30 dB. This means a high polarization purity.

Based on the gain values presented in Table 3, the R-QTL reflectarray achieves a gain that is about 1 dB lower than the one achieved in the R-RRL and R-RTL cases but more stable in-band. The loss of gain at the central frequency for R-QTL is produced by a constrain on the maximum dipole length introduced in the design of reflectarray elements. This is required to avoid overlapping between dipoles of adjacent cells and limits the achievable phase-shift range. Fig. 12 shows the gain of the reflectarray prototypes assessed over a wider range of frequencies (from 25 to 34 GHz). Moreover, Table 4 provides the 1dB bandwidth of each antenna calculated considering the gain of each design at 28 GHz. There is a good agreement between the gain predicted and measured for the three reflectarray prototypes. Trends observed in the band evaluated in Table 3 can also be appreciated from 25 to 34 GHz. Both R-RRL and R-RTL designs suffer a noticeable drop in gain as the frequency deviates from 28 GHz, falling to 30 dBi at 34 GHz. Conversely, the R-QTL maintains gain levels of around 32 dBi between

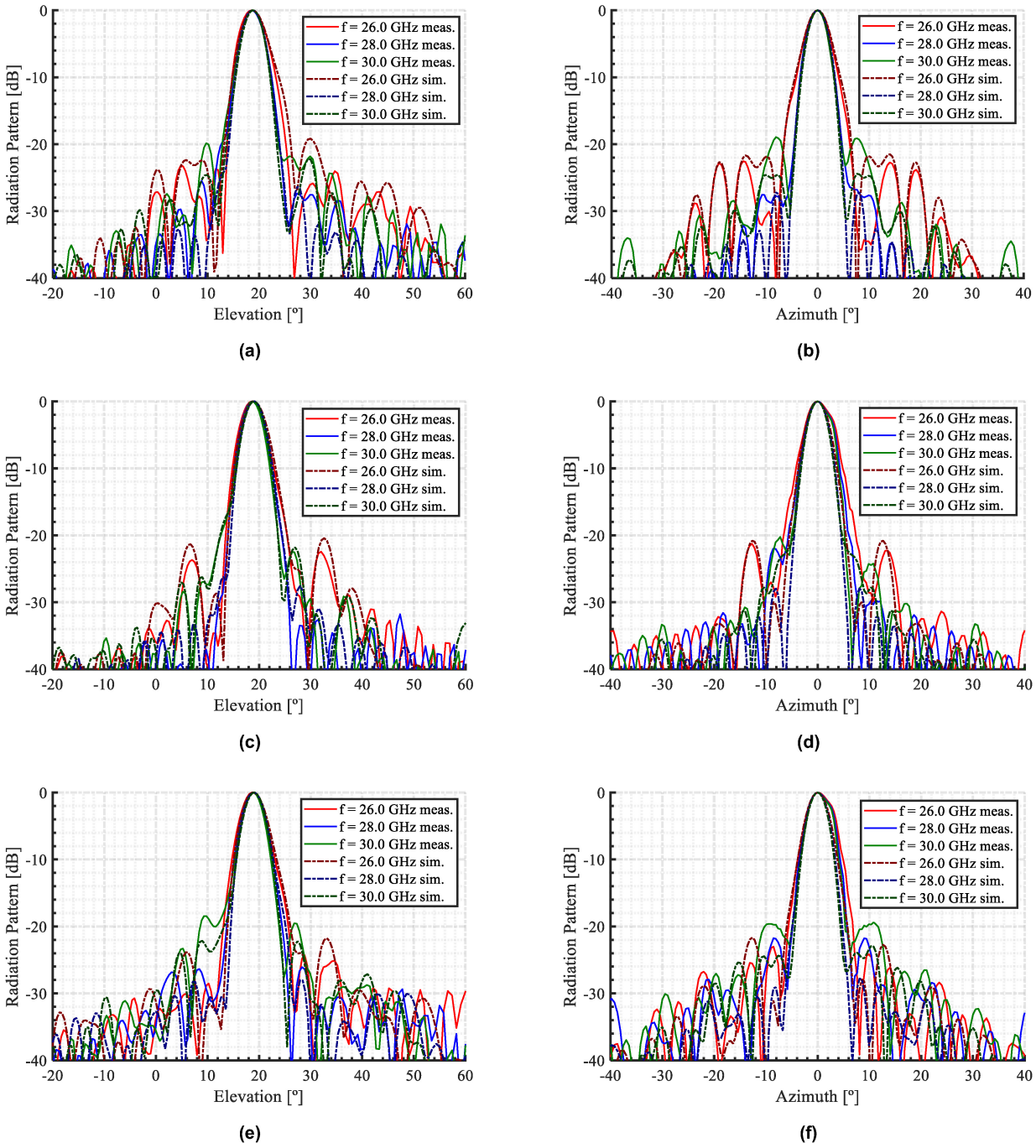

FIGURE 11. Main cuts of normalized radiation pattern in simulation (dotted lines) and measurements (solid lines) for (a), (b) R-RRL reflectarray; (c), (d) R-RTL reflectarray; (e), (f) R-QTL reflectarray. Elevation and Azimuth cuts corresponds to the cut in the spherical coordinates $v = \sin(\theta_0)sin(\varphi_0)$ and $u = \sin(\theta_0)cos(\varphi_0)$, respectively.

27 and 34 GHz, resulting in better in-band performance and antenna bandwidth. Based on the data reported in Table 4, the R-QTL achieves 7.4% and 11.3% more fractional bandwidth than the R-RTL and R-RRL prototypes, respectively.

Since the antenna optics and feed are the same in the three cases, the improvement in the fractional bandwidth is obtained because of the band performance of the reflectarray cells. As the layouts have been designed at 28 GHz, the phase-shift error distribution at 33 GHz is shown for R-RRL and R-QTL in Fig. 13. The error is computed as the difference between the ideal phase shift required to collimate the beam and the phase shift produced by the reflectarray cells at this frequency. It can be appreciated that the error is more constant in the case of R-QTL (see Fig. 13(c)) than for R-RRL (see Fig. 13(b)), mainly in the central part of the

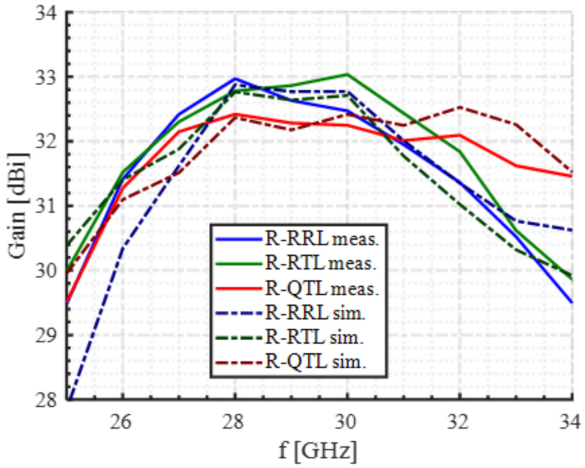

FIGURE 12. Measured copolar gain between 26 to 34 GHz for the three reflectarray designs. Solid lines correspond with measured gain and dotted lines with simulated gain.

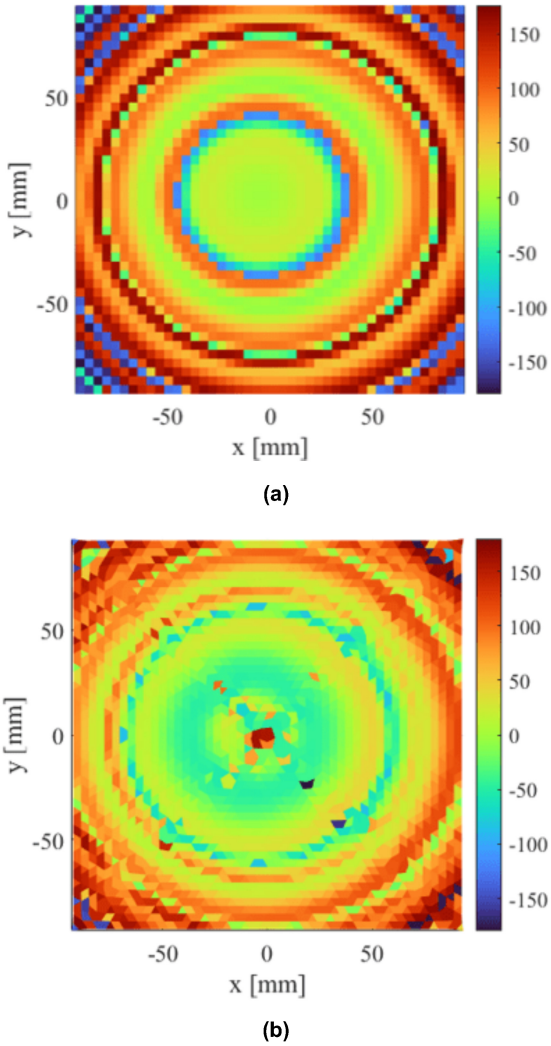

FIGURE 13. Phase-shift error distribution: difference between ideal required phase shift and produced by the reflectarray cells at 33 GHz. (a) R-RRL and (b) R-QTL.

reflectarray where the illumination from the feed is higher. Thus, the beam is less distorted and broader bandwidth is obtained.

VI. CONCLUSION

This work presents some numerical and experimental investigations about the performance of reflectarrays based on quasi-regular element distributions. These element lattices are properly designed to be adapted to the profile of the reflecting aperture. Moreover, a tailored analysis technique has been proposed to evaluate the performance of these antennas. It uses a MoM based on local periodicity to analyze the field on the reflectarray surface under different boundary conditions. The radiated far field of the antenna is computed by dividing the aperture into a set of sub-apertures, whose shapes depend on the element distribution.

Using the proposed analysis technique, two reflectarrays are designed and numerically evaluated. They are based on quasi-regular element distributions and are adjusted to the shape of the reflector. The aperture of these reflectarrays is a rectangle and pentagon respectively, and their performance is compared with two reflectarrays, equivalent in aperture, comprised of regular grids of elements.

The rectangular reflectarray with a quasi-regular lattice, along with its equivalents, has also been evaluated experimentally. The three demonstrators achieve a good agreement between the predicted and the measured results, which validates the proposed analysis technique. The results also demonstrate that the quasi-regular lattice achieves a similar performance compared to the use of a regular lattice of elements in terms of beam shaping, side radiation, and cross-polar isolation. However, it exhibits an improvement of 7.4% and 11.3% of fractional bandwidth compared with triangular and rectangular lattices respectively.

In the pentagonal reflectarray approach, the quasi-regular arrangement exhibits better adaptability to the shape of the aperture than its equivalents based on regular grids. Maintaining a similar inter-element spacing, this lattice achieves higher element density, which enables a finer control of the field in the aperture. The use of a quasi-regular lattice exhibits better in-band performance than the use of regular lattices with similar gain values as the regular triangular lattice and higher than the regular rectangular lattice.

This work validates the proposed technique and demonstrates the capabilities in the use of quasi-periodic lattices adapted to the profile of reflectarray antennas. They allow a more efficient meshing for a reflectarray with an arbitrarily shaped aperture, at the cost of modifying the periodicity conditions imposed in a conventional reflectarray. This adaptability can be further exploited by its application to conformal surfaces.

REFERENCES

[1] G. Minatti et al., "Modulated metasurface antennas for space: Synthesis, analysis and realizations," *IEEE Trans. Antennas Propag.*, vol. 63, no. 4, pp. 1288–1300, Apr. 2015, doi: 10.1109/TAP.2014.2377718.

[2] D. González-Ovejero, G. Minatti, G. Chattopadhyay, and S. Maci, "Multibeam by metasurface antennas," *IEEE Trans. Antennas Propag.*, vol. 65, no. 6, pp. 2923–2930, Jun. 2017, doi: 10.1109/TAP.2017.2670622.

[3] J. Huang and J. A. Encinar, *Reflectarray Antennas*. Hoboken, NJ, USA, Wiley, 2008.

[4] D. Martinez-de-Rioja, R. Florencio, E. Martinez-de-Rioja, M. Arrebola, J. A. Encinar, and R. R. Boix, "Dual-band reflectarray to generate two spaced beams in orthogonal circular polarization by variable rotation technique," *IEEE Trans. Antennas Propag.*, vol. 68, no. 6, pp. 4617–4626, Jun. 2020, doi: 10.1109/TAP.2020.2975294.

[5] B. Imaz-Lueje, D. R. Prado, M. Arrebola, and M. R. Pino, "Reflectarray antennas: A smart solution for new generation satellite mega-constellations in space communications," *Sci. Rep.*, vol. 10, Dec. 2020, Art. no. 21554.

[6] J. R. Reis et al., "FSS-inspired transmitarray for two-dimensional antenna beamsteering," *IEEE Trans. Antennas Propag.*, vol. 64, no. 6, pp. 2197–2206, Jun. 2016, doi: 10.1109/TAP.2016.2543802.

[7] Á. F. Vaquero, M. R. Pino, and M. Arrebola, "Dual-polarized shaped-beam transmitarray to obtain a multizone coverage for 5G indoor communications," *IEEE Antennas Wireless Propag. Lett.*, vol. 21, no. 4, pp. 730–734, Apr. 2022, doi: 10.1109/LAWP.2022.3144365.

[8] O. Koutsos, F. F. Manzillo, A. Clemente, and R. Sauleau, "Design of a 3-bit transmitarray antenna at 300 GHz using asymmetric linear polarizers," in *Proc. IEEE Int. Symp. Antennas Propag. North Amer. Radio Sci. Meeting*, 2020, pp. 1505–1506, doi: 10.1109/IEEECONF35879.2020.9330125.

[9] A. H. Abdelrahman, A. Z. Elsherbeni, and F. Yang, "High-gain and broadband transmitarray antenna using triple-layer spiral dipole elements," *IEEE Antennas Wireless Propag. Lett.*, vol. 13, pp. 1288–1291, 2014, doi: 10.1109/LAWP.2014.2334663.

[10] M. Kartal, J. J. Golezani, and B. Doken, "A triple band frequency selective surface design for GSM systems by utilizing a novel synthetic resonator," *IEEE Trans. Antennas Propag.*, vol. 65, no. 5, pp. 2724–2727, May 2017, doi: 10.1109/TAP.2017.2670230.

[11] K. Fuchi, J. Tang, B. Crowgey, A. R. Diaz, E. J. Rothwell, and R. O. Ouedraogo, "Origami tunable frequency selective surfaces," *IEEE Antennas Wireless Propag. Lett.*, vol. 11, pp. 473–475, 2012, doi: 10.1109/LAWP.2012.2196489.

[12] O. Kiris, K. Topalli, and M. Unlu, "A reflectarray antenna using hexagonal lattice with enhanced beam steering capability," *IEEE Access*, vol. 7, pp. 45526–45532, 2019, doi: 10.1109/ACCESS.2019.2909313.

[13] K. Q. Henderson and N. Ghalichechian, "Triangular and rectangular lattices for cosecant-squared-shaped beam reflectarrays," *IEEE Antennas Wireless Propag. Lett.*, vol. 20, no. 10, pp. 2058–2062, Oct. 2021, doi: 10.1109/LAWP.2021.3103152.

[14] M. M. Mohammadirad, N. Komjani, A. R. Sebak, and M. R. Chaharmir, "A broadband reflectarray antenna using the triangular array configuration," *Appl. Comput. Electromagn. Soc. J.*, vol. 26, no. 8, pp. 640–650, May 2022.

[15] R. W. Kindt and B. T. Binder, "Dual-polarized planar-printed ultrawideband antenna array on a triangular grid," *IEEE Trans. Antennas Propag.*, vol. 68, no. 8, pp. 6136–6144, Aug. 2020, doi: 10.1109/TAP.2020.2972394.

[16] M. Zhou, S. B. Sorensen, O. S. Kim, E. Jorgensen, P. Meincke, and G. Toso, "The generalized direct optimization technique for printed reflectarrays," *IEEE Trans. Antennas Propag.*, vol. 62, no. 4, pp. 1690–1700, Apr. 2014, doi: 10.1109/TAP.2013.2254446.

[17] B. Fuchs, "Synthesis of sparse arrays with focused or shaped beampattern via sequential convex optimizations," *IEEE Trans. Antennas Propag.*, vol. 60, no. 7, pp. 3499–3503, Jul. 2012, doi: 10.1109/TAP.2012.2196951.

[18] T. Clavier et al., "A global-local synthesis approach for large non-regular arrays," *IEEE Trans. Antennas Propag.*, vol. 62, no. 4, pp. 1596–1606, Apr. 2014, doi: 10.1109/TAP.2013.2284816.

[19] A. Capozzoli, C. Curcio, A. Liseno, G. D'Elia, P. Vinetti and G. Toso, "Method for manufacturing an aperiodic array of electromagnetic scatterers, and reflectarray antenna," U.S. Patent 9 742 073 B2, 2011.

[20] R. Sammeta and D. S. Filipovic, "Quasi frequency-independent increased bandwidth planar log-periodic antenna," *IEEE Trans. Antennas Propag.*, vol. 62, no. 4, pp. 1937–1944, Apr. 2014, doi: 10.1109/TAP.2014.2302001.

[21] M. K. T. Al-Nuaimi, W. Hong, and W. G. Whittow, "Aperiodic sunflower-like metasurface for diffusive scattering and RC1S reduction," *IEEE Antennas Wireless Propag. Lett.*, vol. 19, no. 7, pp. 1048–1052, Jul. 2020, doi: 10.1109/LAWP.2020.2980906.

[22] M. W. Niaz, Z. Ahmed, and M. B. Ihsan, "Reflectarray with logarithmic spiral lattice of elementary antennas on its aperture," *Int. J. Electron. Commun.*, vol. 70, no. 8, pp. 1050–1054, 2016, doi: 10.1016/j.aeue.2016.04.020.

[23] A. J. Rubio, A.-S. Kaddour, C. Ynchausti, S. Magleby, L. L. Howell, and S. V. Georgakopoulos, "A foldable reflectarray on a hexagonal twist origami structure," *IEEE Open J. Antennas Propag.*, vol. 2, pp. 1108–1119, 2021, doi: 10.1109/OJAP.2021.3127312.

[24] C. A. Velez, A.-S. Kaddour, S. V. Georgakopoulos, C. Ynchausti, S. Magleby, and L. L. Howell, "A novel miura-ori origami reflectarray antenna for CubeSat applications," in *Proc. IEEE Int. Symp. Antennas Propag. USNC-URSI Radio Sci. Meeting (APS/URSI)*, 2021, pp. 1759–1760, doi: 10.1109/APS/URSI47566.2021.9704247.

[25] B. Imaz-Lueje, M. R. Pino, and M. Arrebola, "Deployable multi-faceted reflectarray antenna in offset configuration with band enhancement," *IEEE Trans. Antennas Propag.*, vol. 70, no. 12, pp. 11686–11696, Dec. 2022, doi: 10.1109/TAP.2022.3209753.

[26] A.-S. Kaddour et al., "A foldable and reconfigurable monolithic reflectarray for space applications," *IEEE Access*, vol. 8, pp. 219355–219366, 2020, doi: 10.1109/ACCESS.2020.3042949.

[27] C. Wan and J. A. Encinar, "Efficient computation of generalized scattering matrix for analyzing multilayered periodic structures," *IEEE Trans. Antennas Propag.*, vol. 43, no. 11, pp. 1233–1242, Nov. 1995, doi: 10.1109/8.475095.

[28] R. Florencio, R. R. Boix, and J. A. Encinar, "Efficient spectral domain MoM for the design of circularly polarized reflectarray antennas made of split rings," *IEEE Trans. Antennas Propag.*, vol. 67, no. 3, pp. 1760–1771, Mar. 2019, doi: 10.1109/TAP.2018.2888956.

[29] A. Gómez-Álvarez, B. Imaz-Lueje, D. R. Prado, M. Arrebola, and M. R. Pino, "Comparative study of different approaches to analyze unit cells of reflectarray antennas" in *Proc. 15th Eur. Conf. Antennas Propag. (EuCAP)*, 2021, pp. 1–4.

[30] W. L. Stutzman and G. A. Thiele, *Antenna Theory and Design*, 3rd ed. Hoboken, NJ, USA: Wiley, 2012.

[31] Á. F. Vaquero, M. Arrebola, M. R. Pino, R. Florencio, and J. A. Encinar, "Demonstration of a reflectarray with near-field amplitude and phase constraints as compact antenna test range probe for 5G new radio devices," *IEEE Trans. Antennas Propag.*, vol. 69, no. 5, pp. 2715–2726, May 2021, doi: 10.1109/TAP.2020.3030969.

[32] A. K. Bhattacharyya, *Phased Array Antennas*. Hoboken, NJ, USA: Wiley, 2006.

[33] A. Capozzoli, C. Curcio, A. Liseno, and G. Toso, "Fast and phase-only synthesis of aperiodic reflectarrays using a NUFFTs and CUDA," *Progr. Electromagn. Res.*, vol. 156, pp. 83–103, Jun. 2016.

[34] A. Capozzoli, C. Curcio, and A. Liseno, "Optimized nonuniform FFTs and their application to array factor computation," *IEEE Trans. Antennas Propag.*, vol. 67, no. 6, pp. 3924–3938, Jun. 2019, doi: 10.1109/TAP.2018.2826368.

[35] R. Mittra, C. H. Chan, and T. Cwik, "Techniques for analyzing frequency selective surfaces–A review," *Proc. IEEE*, vol. 76, no. 12, pp. 1593–1615, Dec. 1988.

[36] J. Córcoles and R. R. Boix, "Spectral MoM NUFFT-Based formulation for the efficient analysis of high-order bandpass FSSs with tightly packed nonresonant elements in skewed grid," *IEEE Trans. Antennas Propag.*, vol. 69, no. 9, pp. 6099–6104, Sep. 2021.

[37] A. M. Lerer and A. G. Schuchinsky, "Full-wave analysis of three-dimensional planar structures," *IEEE Trans. Microw. Theory Techn.*, vol. 41, no. 11, pp. 2002–2015, Nov. 1993.

[38] M. K. Loze and R. Saunders, "Two simple algorithms for constructing a two-dimensional constrained Delaunay triangulation," *Appl. Numer. Math.*, vol. 11, no. 5, pp. 403–418, 1993.

[39] P. L. George, *Automatic Mesh Generation: Application to Finite Element Methods*. Hoboken, NJ, USA: Wiley, 1991.

[40] "TICRA: GRASP | Reflector antenna design software." Accessed: Aug. 1, 2023. [Online]. Available: https://www.ticra.com/software/grasp/

[41] "TICRA: SNIFT | Spherical near-field transformation software." Accessed: Aug. 1, 2023. [Online]. Available: https://www.ticra.com/software/snift/

BORJA IMAZ-LUEJE (Student Member, IEEE) was born in Asturias, Spain, in 1995. He received the B.Sc., M.Sc., and Ph.D. degrees in telecommunication engineering from the Universidad de Oviedo (UO), Gijón, Spain, in 2017, 2019, and 2023, respectively.

Since 2016, he has been a Research Assistant with the Electrical Engineering Department, UO. From 2018 to 2019, he spent several months in Rohde & Schwarz GmbH & Co KG, Munich, Germany, where he was involved in the deployment of CATR systems and OTA measurements. In 2022, he was in a research mission with Institut d'Electronique et des Technologies du numeRique, Rennes, France, where he was involved in the analysis and design of compact antennas. His current research interests include the development of efficient analysis and design techniques of reflectarrays in complex configurations, working in environments of near and far field.

JUAN CÓRCOLES (Senior Member, IEEE) was born in Albacete, Spain, in 1981. He received the Ingeniero de Telecomunicación (B.Sc. and M.Sc.) degrees in electrical engineering and the Ph.D. degree from the Universidad Politécnica de Madrid, Spain, in 2004 and 2009, respectively.

Since 2010, he has been with the Universidad Autónoma de Madrid, Spain, where he became an Associate Professor in 2015. His current research interests are in applied and computational electromagnetics, particularly in the development of numerical methods and optimization techniques for the analysis and design of microwave circuits, antennas, and other related applications.

MARCOS R. PINO received the M.Sc. and Ph.D. degrees in telecommunication engineering from the University of Vigo, Spain, in 1997 and 2000, respectively.

In 1998, he was a Visiting Scholar with the ElectroScience Laboratory, The Ohio State University, Columbus, OH, USA. From 2000 to 2001, he was an Assistant Professor with the University of Vigo. Since 2001, he has been with the Electrical Engineering Department, University of Oviedo, Gijón, Spain, where he is currently a Full Professor, teaching courses on communication systems and antenna design. From 2017 to 2019, he has spent several months as a Visiting Fellow with the Department of Information Engineering, University of Pisa, Italy, collaborating in near-field UHF-RFID applications. His current research interests include antenna design optimized for both near-field and far-field applications, antenna measurement techniques, and efficient computational techniques applied to EM problems.

MANUEL ARREBOLA (Senior Member, IEEE) was born in Lucena, Spain. He received the M.Sc. degree in telecommunication engineering from the Universidad de Málaga, Málaga, Spain, in 2002, and the Ph.D. degree in electrical engineering from the Universidad Politécnica de Madrid (UPM), Madrid, Spain, in 2008.

From 2003 to 2007, he was a Research Assistant with the Department of Electromagnetism and Circuit Theory, UPM. He was a Visiting Researcher with the Department of Microwave Techniques, Universität Ulm, Ulm, Germany. In 2007, he joined the Department of Electrical Engineering, Universidad de Oviedo, Gijón, Spain, where he is currently an Associate Professor with the Signal Theory and Communications Group. In 2009, he was with the European Space Research and Technology Centre, European Space Agency, Noordwijk, The Netherlands, as a Visiting Researcher. He has been a Visiting Professor with several institutions, such as the Edward S. Rogers Sr. Department of Electrical and Computer Engineering, University of Toronto, Toronto, ON, Canada, in 2018; the Institute of Sensors, Signals and Systems, Heriot-Watt University, Edinburgh, U.K., in 2019; and the Antennas and Propagation Group, Instituto de Telecomuncações, Lisbon, Portugal, in 2023. He has authored and coauthored more than 200 peer-reviewed journals and conference papers. His current research interests include the application of innovative manufacturing techniques in mm and sub-mmWave antenna design, and the development of efficient analysis, design, and optimization techniques of spatial fed arrays, including reflectarrays and transmitarrays and periodic structures for near- and far-field applications.

Dr. Arrebola was a co-recipient of the 2007 Sergei A. Schelkunoff Transactions Prize Paper Award from the IEEE Antennas and Propagation Society. He has also received the 2008 Outstanding Ph.D. Thesis Award from UPM and the 2009 National Award for the Best Ph.D. Thesis on Telecommunication Networks and Services. Since 2022, he has been an Associate Editor of the IEEE TRANSACTIONS ON ANTENNAS AND PROPAGATION.